

# Chaotic diffusion in the 2/1 asteroidal resonance

## An application of the frequency map analysis

D. Nesvorný\* and S. Ferraz-Mello

Instituto Astronômico e Geofísico, Universidade de São Paulo, Caixa Postal 9638, CEP 04301, São Paulo, Brasil

Received 29 August 1996 / Accepted 19 September 1996

**Abstract.** We have applied the frequency map analysis of Laskar (1993) to the following dynamical models of the 2/1 asteroidal mean-motion resonance: the planar restricted three-body model and the planar restricted four-body model with Saturn. It allowed us to reproduce the chaotic region, which is formed by the overlap of secondary resonances in low eccentricities. We have examined the chaos generated by high-order secondary resonances in moderate eccentricities and concluded that, in the three-body planar model, most of the area remains regular even in the model with Jupiter's eccentricity equal to 0.061. But, when the basic secular frequencies of Jupiter's orbit were taken into account, the moderate-eccentricity region turned chaotic and a slow chaotic diffusion appeared. The diffusion was found to be more significant in the full, planar four-body model. Asteroids exhibited random excursions in the phase space and we studied this possible mechanism of resonance emptying in several 10-Myr integrations.

**Key words:** minor planets – celestial mechanics – chaos

### 1. Introduction

The 2/1 asteroidal mean-motion resonance with Jupiter coincides with the Hecuba gap. Until now, no complete explanation of the origin of this gap exists. Apart from cosmogonic conjectures, the most promising is the hypothesis that asteroids initially present in the resonant region were transferred to the high-eccentricity or Jupiter approaching orbits and were consequently ejected from the resonance.

Giffen (1973) discovered the chaotic motion in low eccentricities of the 2/1 resonance. This chaotic region was found to be confined to the low eccentricities in the three-body planar model, but numerical integrations with the four major planets (Wisdom 1987) showed escapes to high eccentricities and sug-

gested a possible way of how the low-eccentricity chaotic region was emptied.

Lemaître & Henrard (1990) explained the existence of the chaotic zone in low eccentricities by the overlap of secondary resonances involving the circulation of longitude of perihelion  $\varpi$  and the libration of critical angle

$$\sigma = 2\lambda_J - \lambda - \varpi \quad (1)$$

( $\lambda$  and  $\lambda_J$  are mean longitudes of a resonant asteroid and Jupiter). Morbidelli & Moons (1993) studied the effect of secular perturbations of Jupiter's orbit. They found the chaotic motion generated by the secular resonances  $\nu_5$  and  $\nu_6$  near separatrices of the 2/1 resonance and in high eccentricities. In the case of  $\nu_{16}$ , they showed that, although placed near the libration centers, it does not provide any mechanism for transition to the high eccentricities.

Ferraz-Mello (1994) calculated a set of the Poincaré diagrams of the restricted, planar and averaged three-body problem clearly showing the confinement of the low-eccentricity chaotic region by regular trajectories. Moreover, he studied the spatial four-body model with Saturn. His computation of the maximum Lyapunov exponent (MLE) for a representative sample of initial conditions showed that the whole 2/1 asteroidal resonance is dominated by chaos. Typical Lyapunov times (inverse of MLE) were found between  $10^4$  and  $10^6$  years. This result raised a question whether the slow chaotic diffusion present in the model with Saturn led to significant transitions in the phase space during the solar system existence.

A recent paper of Henrard et al. (1995) explained Wisdom's integration. They localized a bridge between the secondary and secular resonances at inclinations  $\sim 25$  deg allowing a random walk from the low to high eccentricities. But even this detailed work did not answer completely the question of the Hecuba gap origin. They concluded: 'Orbits starting with small amplitude of libration, small inclination and eccentricities between 0.25 and 0.45 do not seem to have many possibilities to evolve. There are no resonances there except very high order resonances and the evolution through Arnold diffusion should be very, very slow.' A study of the chaotic diffusion in the moderate-eccentricity region is a main objective of this article.

---

Send offprint requests to: D. Nesvorný

\* e-mail address: david@vax.iagusp.usp.br

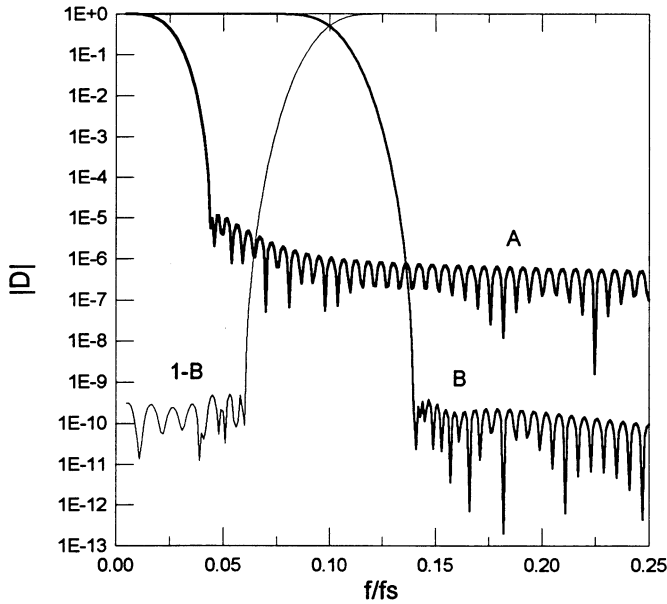


**Fig. 1.** Fourier transforms of the filters A and B described in Quinn et al. (1991), the thin line is  $1 - |D|$  of B where the ripple as well as the limit of passband are visible (sampling frequency  $f_s$  is defined by  $f_s = 1/\Delta$ , where  $\Delta$  is the sampling interval)

A suitable tool for such a task is the frequency map analysis (FMA) introduced by Laskar (1990). This technique is based on a numerical calculation of frequencies, which do not depend on time in a regular system but are time-dependent in a chaotic system. The chaotic diffusion is then measured through time evolution of the determined frequencies. The most detailed overview of FMA was given in Laskar (1993).

## 2. The technique

The equations of motion of the restricted four-body model (Sun - Jupiter - Saturn - asteroid) are

$$\ddot{\mathbf{r}} = -Gm_{\odot} \frac{\mathbf{r}}{r^3} + G \sum_{i=1}^2 m_i \left( \frac{\mathbf{r}_i - \mathbf{r}}{|\mathbf{r}_i - \mathbf{r}|^3} - \frac{\mathbf{r}_i}{r_i^3} \right), \quad (2)$$

where  $G$  is the gravitational constant,  $m_{\odot}$  is the mass of the Sun,  $m_1$  and  $m_2$  are the masses of Jupiter and Saturn,  $\mathbf{r}$ ,  $\mathbf{r}_1$  and  $\mathbf{r}_2$  are the heliocentric position vectors of the asteroid, Jupiter and Saturn.

We have performed an extensive number of numerical integrations of Eq. (2) (system Sun-Jupiter-Saturn has been propagated by a parallel integration of the three-body model) using the symmetric multistep method of Quinlan & Tremaine (1990). Although slower than the step-variable integrator RA-15 of Everhart (1985), especially at higher eccentricities, this method is of better precision due to the reduced error propagation. The integrator has the form

$$x_{n+1} = - \sum_{j=1}^k \alpha_{k-j} x_{n-j+1} + h^2 \sum_{j=1}^k \beta_{k-j} f_{n-j+1}, \quad (3)$$

where  $x_n$  is the Cartesian coordinate at step  $n$ ,  $f_n$  is a corresponding component of the acceleration computed by Eq. (2),  $h$  is a fixed stepsize and  $\alpha_j, \beta_j$  are coefficients of the method. We used the symmetric method with  $k = 12$  (SMU12), which has  $\alpha_j = \alpha_{k-j}, \beta_j = \beta_{k-j}, \alpha_0 = 1$  and  $\beta_0 = 0$ . The coefficients were chosen so that a 13th-order polynomial is integrated exactly.

We have tested a precision of the integrator in the two-body Keplerian problem. A comparison with the Störmer method (Cohen et al. 1973) has shown better stability properties of the symmetric method in higher eccentricities. For example, a step of 10 days leads to the reasonable relative errors  $4 \times 10^{-6}$  in semi-major axis and  $7 \times 10^{-4}$  in mean longitude after 1 Myr for eccentricity  $e = 0.5$  and orbit at the 2/1 resonance (a stepsize-period ratio of  $\sim 2.5 \times 10^{-4}$ ) with SMU12 while the Störmer method is unstable there. The Runge-Kutta method of the 4th-order with small stepsize has been used to start SMU12. This is as accurate as the starting iterator of Cohen et al. (1973).

An effective procedure of a memory management requires a digital low-pass filter. We used two digital filters called A and B which are described in Quinn et al. (1991). The filter A has ripple  $3.5 \times 10^{-5}$ , suppression  $10^{-5}$ , limits of passband and stopband 0.005 and 0.05, respectively. The filter B has, similarly, ripple  $10^{-9}$ , suppression  $10^{-9}$ , passband 0.05 and stopband 0.15. See Press et al. (1992) for a definition of these characteristic parameters.

Data  $w$  with a certain sampling on the filter input are replaced by  $w'$  on the output following the convolution relation,

$$w'_n = \sum_{m=-M}^M d_m w_{n-m}, \quad (4)$$

where  $d_m$  are coefficients of the filter with length  $2M + 1$ . The discrete Fourier transform of this relation gives

$$W'_n = D_n W_n, \quad (5)$$

where  $W'_n, W_n$  and  $D_n$  denote transforms of  $w'_n, w_n$  and  $d_n$ . Fig. 1 shows the Fourier transforms  $D_n$  of both filters.

As a result we get the low-band limited signal  $W'_n$ , which allows us to increase the sampling. The typical value was a decimation by the factor 6, from the initial spacing of 2 yr to 12 yr. It means, when working with the filter A, that the frequencies smaller than 40 yr were removed and the frequencies larger than 400 yr were retained. For the filter B, which had to be applied sequentially two times, these values were 40 yr and 120 yr.

The basic frequencies, which appear in the spectrum of asteroid's osculating elements, are the libration frequency  $f_{\sigma}$  of the critical argument  $\sigma$  (characteristic period of several hundreds of years) and the circulation frequency  $f_{\varpi}$  of the longitude of perihelion  $\varpi$  (thousands to tens of thousand years). See Michtchenko & Ferraz-Mello (1995) for an overview of this subject.

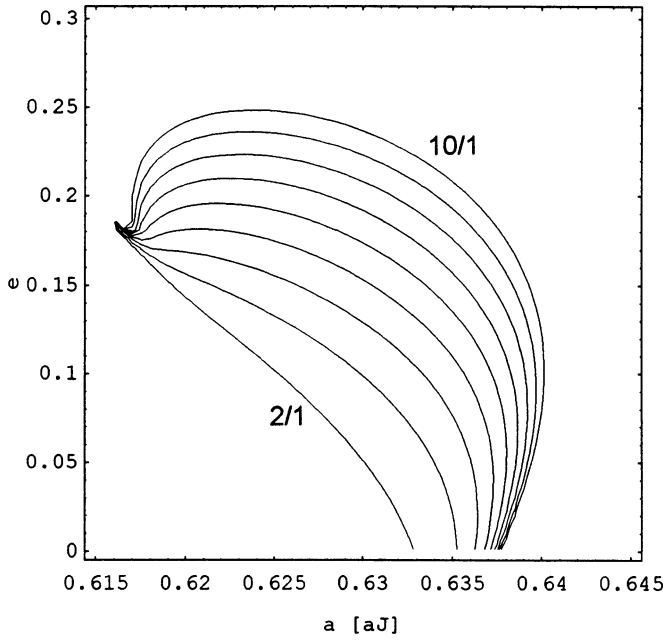


**Fig. 2.** The secondary resonances calculated by the semi-numerical method

The frequencies were determined by Laskar's technique (Laskar et al. 1992). One defines a scalar product of two functions  $f(t)$  and  $g(t)$  on the interval  $-T \leq t \leq T$  by

$$\langle f, g \rangle = \frac{1}{2T} \int_{-T}^T f(t) \bar{g}(t) \chi(t) dt, \quad (6)$$

where  $\chi(t) = 1 + \cos(\pi t/T)$  is the Hanning window. If  $f(t)$  is singly periodic,  $f(t) = a_1 e^{i\omega_1 t}$ , where  $a_1$  is a complex amplitude and  $\omega_1$  is a frequency, then a modulus of the function  $\phi(\omega)$  defined by

$$\phi(\omega) = \langle f(t), e^{i\omega t} \rangle \quad (7)$$

has a maximum at  $\omega_1$  and  $\phi(\omega_1) = a_1$ . Thus, having the values of  $f$  regularly spaced over the  $2T$ -interval as an output of numerical simulation, we numerically compute the maximum of  $|\phi|$  and obtain the frequency  $\omega_1$ .

In a general case, where  $f$  includes an infinite number of periodic terms, we perform Laskar's iterative process, which is stopped when a desired number of frequencies is obtained or if, at a certain step, the new frequency falls closer than  $\pi/T$  to any already determined one. As a result, we get  $n$  frequencies separated by more than  $\pi/T$ . Amplitudes  $a_k$ ,  $k = 1, \dots, n$  obtained by the final projection complete the reconstruction  $f'$  of the function  $f$ :  $f'(t) = \sum_{k=1}^n a_k e^{i\omega_k t}$ .

This representation is not exact and an error, which originates from overlapping of different terms in  $\phi$ , is estimated in the following way. We sample the function  $f'$  and reconstruct its representation  $f'' = \sum_{k=1}^n a'_k e^{i\omega'_k t}$ . The differences between frequencies  $|\omega_k - \omega'_k|$  and amplitudes  $|a_k - a'_k|$  can be considered to be the overlap errors of the representation  $f'$  (Laskar et al. 1992).

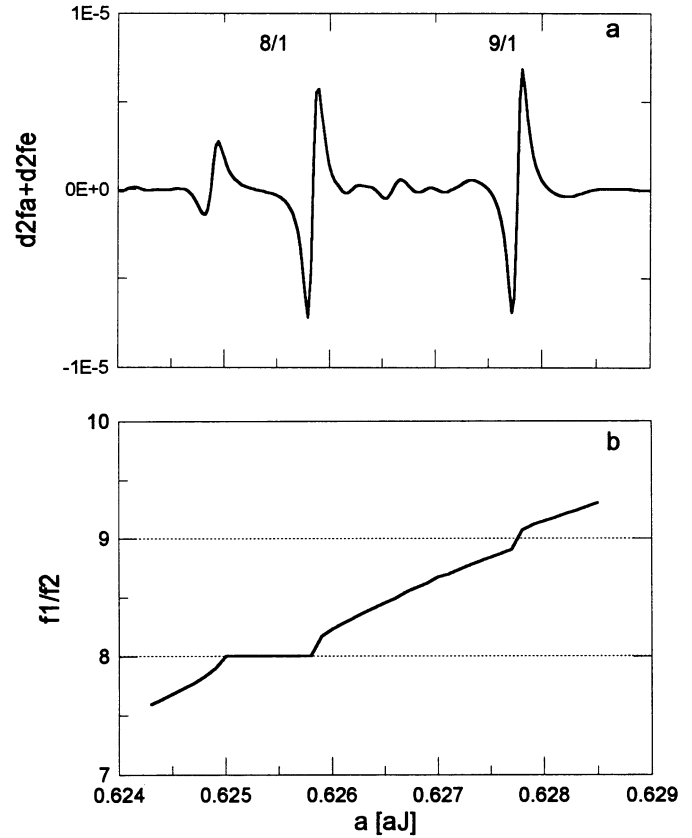


**Fig. 3a and b.** The second derivative singularities of the frequency  $f_\sigma$  at separatrix crossings and the ratio  $f_\sigma/f_\omega$

Our extension of Laskar's error estimation is the following. A final error is calculated as composed from the overlap error and an error 'due to residuals' left in the given peak. As an error of the amplitude, we take  $\max(a_{\text{res}}, \delta|a|)$ , where  $a_{\text{res}}$  is a maximum of the spectra between  $f_\omega - \pi/T$  and  $f_\omega + \pi/T$  after the subtraction of all determined terms. In order to estimate the frequency error due to the residuals, we imagine a sum of the function

$$\begin{aligned} \phi(\omega) &= \langle a_\omega e^{if_\omega t}, e^{i\omega t} \rangle = \\ &= -a_\omega \frac{\sin(\omega - f_\omega)T}{(\omega - f_\omega)T} \frac{\pi^2}{[(\omega - f_\omega)^2 T^2 - \pi^2]} \end{aligned} \quad (8)$$

and some unknown function with the maximum value  $a_{\text{res}}$ . The  $\phi$  can be approximated by  $\phi'(\omega) = a_\omega (1 + bT^2(\omega - f_\omega)^2)$  near  $f_\omega$ , where  $b = (\pi^2 - 6)/6\pi^2$ , and the condition  $\phi'(\omega) = a_\omega - a_{\text{res}}$  gives the maximum frequency distance where a false absolute maximum can appear:

$$\sqrt{\frac{6\pi^2}{\pi^2 - 6}} \sqrt{\frac{a_{\text{res}}}{a_\omega}} \frac{1}{T}. \quad (9)$$

This expression can be seen as an upper estimate of the error due to residuals. Thus, the final frequency error is computed as a maximum of  $\delta f$  and Eq. (9).

Now, for a chaotic trajectory, where a change of frequency determined for different time periods is expected, the error es-

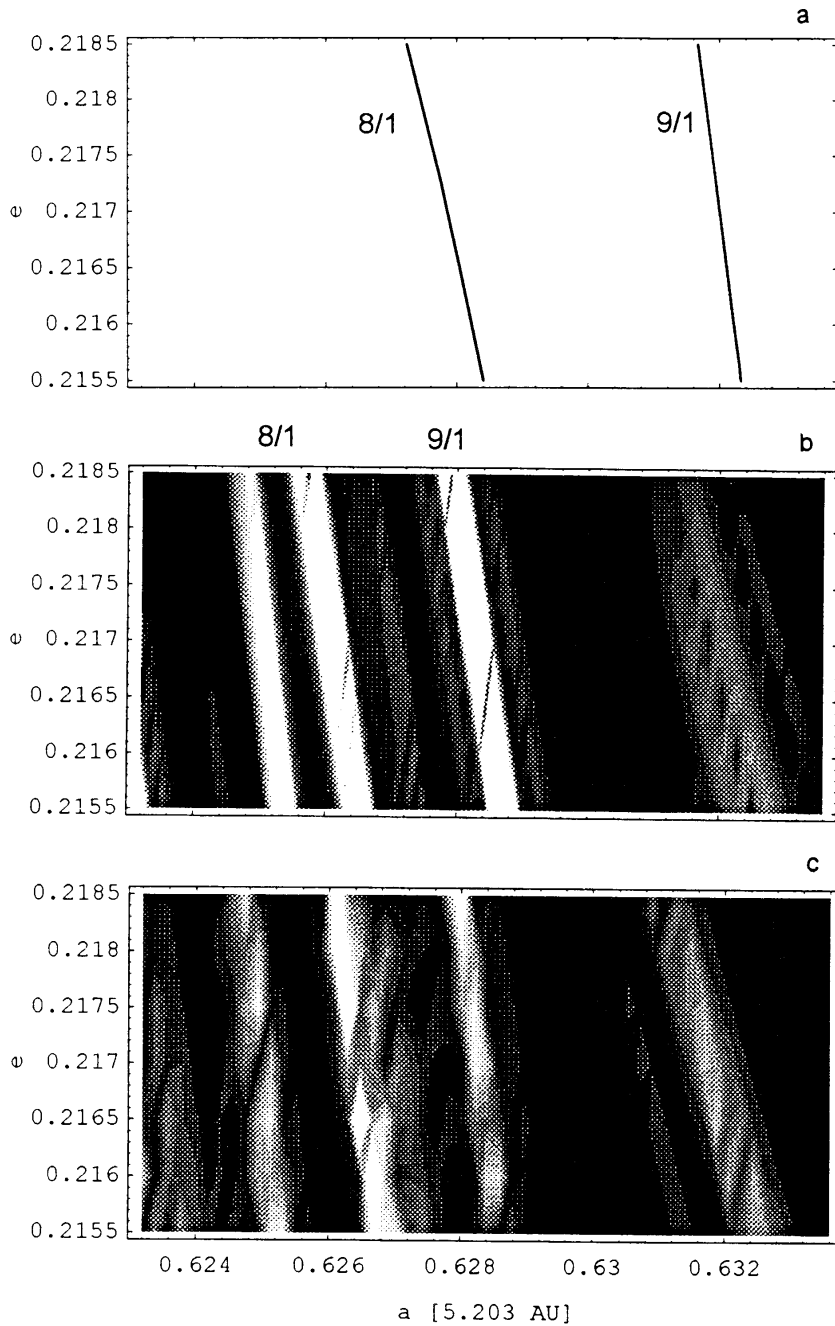


**Fig. 4a-c.** Position of the secondary resonances in three models: circular **a**, elliptic **b** and with Saturn **c**

timation gives us the following criterion for adjusting of  $T$  and an offset (the time interval separating two frequency determinations): If, for certain  $T$ , the estimated error is larger than or comparable with the observed frequency change over the given offset, the time  $T$  must be enlarged and/or longer offset should be used, and only if the error is apparently smaller than the frequency change, the chaoticity of the trajectory is affirmed. The frequencies and amplitudes should be fixed in the case of a regular trajectory and sufficiently long  $T$ .

The error analysis is important since it is necessary to reduce the timespan of integrations as much as possible in order to be

able to extend the frequency calculations to a large number of initial conditions.

The frequency  $f_{\omega}$  is calculated as the strongest peak in the spectrum of  $e(t)e^{i\omega(t)}$  ( $e$  is eccentricity). The frequency  $f_{\sigma}$  is evaluated in a more complicated way since it is not easy to define any phase-space variable in which the spectral peak  $f_{\sigma}$  always dominates (Michtchenko & Ferraz-Mello 1996). We determine several peaks in spectra and choose the one which is the nearest to the libration frequency of  $\sigma$  in the three-body circular model.

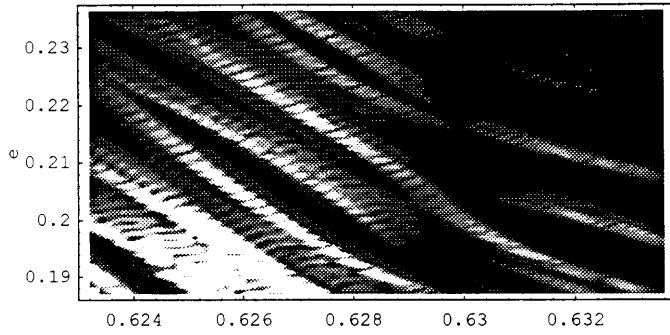


Fig. 5. The secondary resonances in the four-body planar model

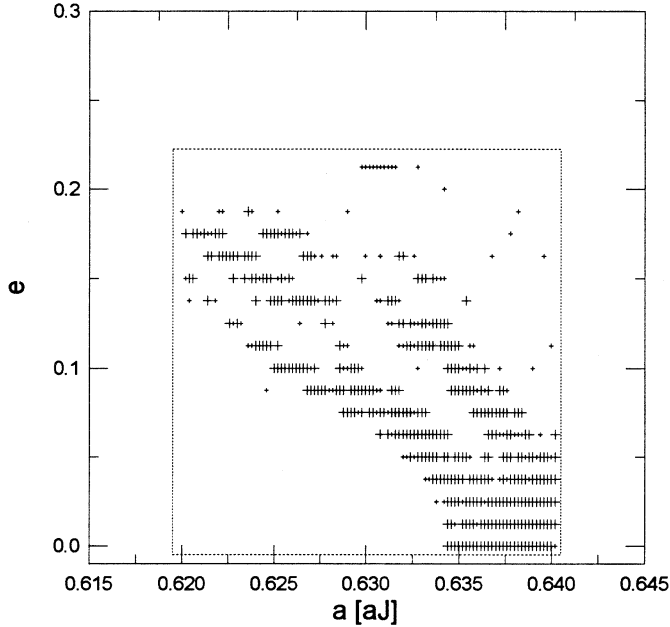


Fig. 6. The chaotic region in low eccentricities

### 3. Secondary resonances

Following the semi-numerical method of Lemaître & Henrard (1990) and using the Ferraz-Mello & Sato (1989) evaluation of the perturbing function, as it was done in Moons & Morbidelli (1993), we have computed a position of several secondary resonances in the planar and circular three-body model. The lowest and the highest-order secondary resonances are denoted by a corresponding ratio  $f_\sigma/f_\omega$  in Fig. 2. The high-order secondary resonances reach the moderate eccentricity region and, in the forthcoming analysis, we will be interested in their exact position in the elliptic and four-body planar models.

The behaviour of frequencies at the secondary resonances is shown in Fig. 3a and b. In Fig. 3a we have plotted a numerical estimate of  $\frac{\partial^2 f_\omega}{\partial a^2} + \frac{\partial^2 f_\omega}{\partial e^2}$  for the set of initial conditions  $e = 0.217$ ,  $\varpi = 0$ ,  $\lambda = 0$  and  $a$  between 0.624 and 0.629  $a_J$  (3.2467 and 3.2727 AU for  $a_J = 5.203$  AU), computed in the planar elliptic three-body model by the technique described in Sect. 2. The three discontinuities at approximately 0.6249, 0.6258 and 0.6278  $a_J$  appear at separatrices of the secondary resonances.

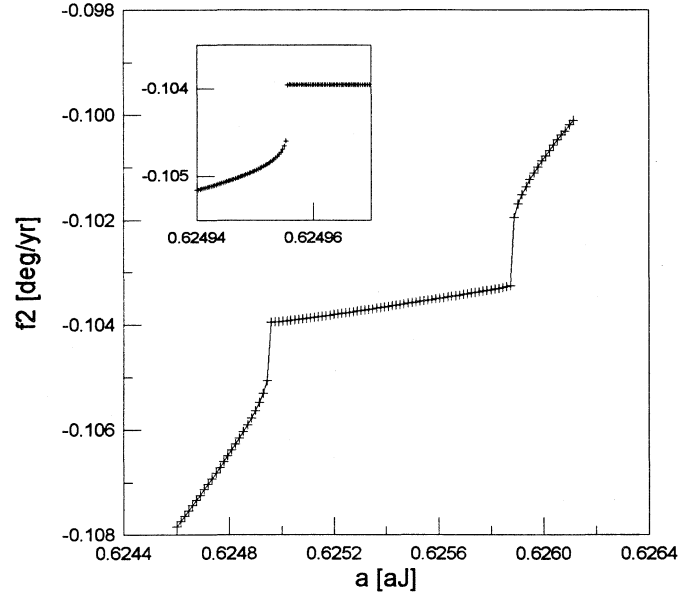


Fig. 7. The 8/1 secondary resonance

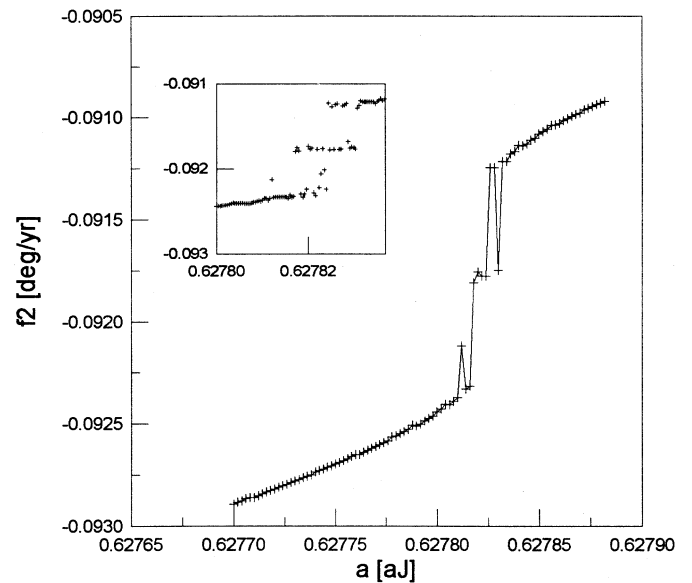


Fig. 8. The 9/1 secondary resonance

We identified by evaluation of  $f_\sigma$  that the first two correspond to the 8/1 and the later to the 9/1 secondary resonances. In between the first and the second discontinuity, the frequencies  $f_\sigma$  and  $f_\omega$  are locked in a precise ratio of 8/1 (Fig. 3b). This plateau, which is typical for the elliptic point crossing, as well as the hyperbolic point crossing at 9/1, is associated with chosen  $e = 0.2168$ . Other initial values of  $e$ ,  $e \sim 0.225$  for instance, lead to the hyperbolic point crossing at 8/1.

The frequency  $f_\omega$  for the estimate of the derivative in (a) was calculated from only  $2T = 3.2 \times 10^4$  yr, what led to a slight distortion of the frequency curve. In fact, if  $T$  is longer, as it was done in (b) where  $2T = 4 \times 10^5$  yr, the second derivative is equal to zero inside the libration island.

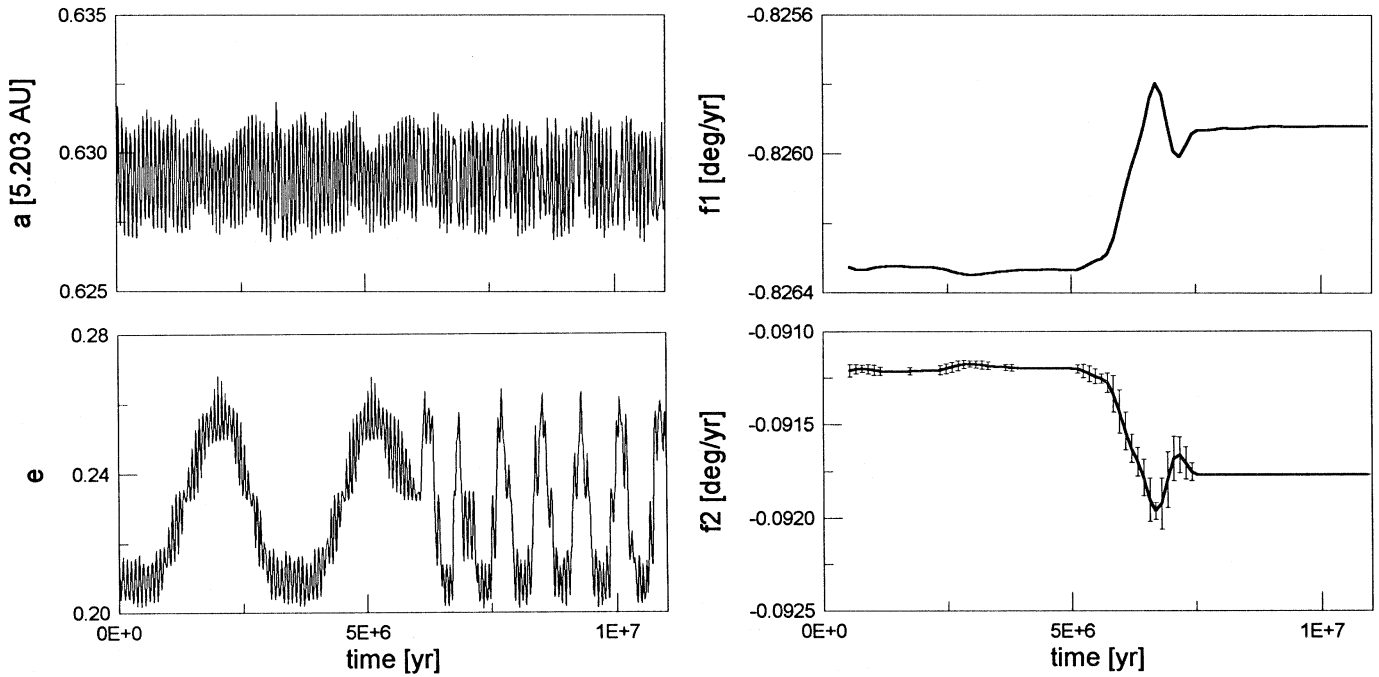


Fig. 9. The chaotic trajectory in the 9/1 secondary resonance

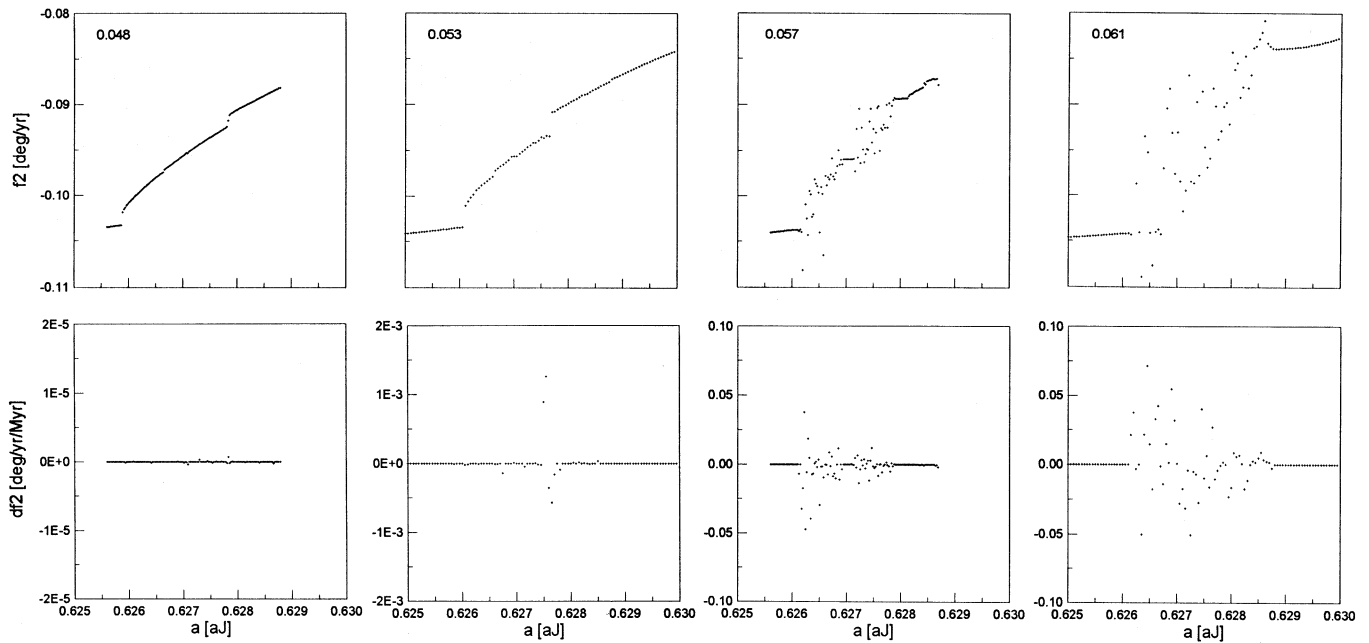


Fig. 10. The sensitivity of the model to Jupiter's eccentricity for  $e = 0.2168$

Fig. 4a–c is a comparison of the secondary resonances position in three planar models: (a) is the circular three-body model, (b) is the elliptic three-body model ( $e_J = 0.048$ ) and in (c), the effect of Saturn was included. Each rectangle is a narrow strip centered at the eccentricity 0.217. (a) is in fact a small part of Fig. 2, the result of the semi-numerical method. The bright strips in (b) and (c) are the places of the separatrix crossings seen in Fig. 3a. We have made integrations spanning  $3.2 \times 10^4$  yr for a fine net of initial conditions inside the shown rectangles with

spacing 0.0005 in eccentricity and 0.0002  $a_J$  in semi-major axis (zero initial angles) and, similarly as in Fig. 3, we have computed the value of  $|\frac{\partial^2 f_{\varpi}}{\partial a^2}| + |\frac{\partial^2 f_{\varpi}}{\partial e^2}|$ . Now, the bright areas in (b) and (c) are the places where this quantity has a high value, which shows an approximate position of the separatrices. In the elliptic and four-body models the 8/1 and 9/1 secondary resonances are shifted to the left in comparison to the circular model, which means to lower values of the semi-major axis. They are close to-

gether and the 8/1 secondary resonance apparently broadens in the four-body model. Moreover, the 10/1 secondary resonance appears on the right. The 8/1 secular resonance has an elliptic island on the studied surface while the 9/1 resonance has a hyperbolic point there. It is clearly visible in Fig. 4b but less clear in Fig. 4c where the resonant borders get fuzzy.

The same computation was extended in the planar four-body model to a larger area of initial conditions in eccentricities. The result is shown in Fig. 5. We see there, going along a diagonal from bottom-left to top-right, the overlapping resonances 6/1 and 7/1 at  $a \sim 0.625 a_J$  (3.25188 AU), a large island of the 8/1 resonance at  $a \sim 0.627 a_J$  (3.26228 AU) and weaker high-order resonances further to the right.

#### 4. The elliptic three-body model

For every initial condition, we have integrated a trajectory in the three-body planar model ( $e_J = 0.048$ ) for  $1.5 \times 10^5$  yr. We have determined the frequency  $f_\varpi$  twice – in two intervals  $10^5$  yr overlapping by one half, that means an offset of  $5 \times 10^4$  yr. The initial conditions were  $0.62 a_J \leq a \leq 0.64 a_J$  and  $0 \leq e \leq 0.225$  (all angles were zero). The initial conditions for which the frequency  $f_\varpi$  changed relatively by more than  $10^{-3}$  over the given offset are marked by big crosses in Fig. 6. Small crosses correspond to the relative changes larger than  $10^{-4}$  and the rest, with almost constant  $f_\varpi$ , is left empty. The chaotic zone that appears along the low-order secondary resonances (see Fig. 2) can be compared to Murray (1986) and Wisdom (1987).

No significant chaotic behaviour exists for  $e = 0.2$  and even for lower eccentricities on the right side of the dotted rectangle. In the planar three-body model the high-order secondary resonances are present in this region but they do not overlap and do not generate a large-scale chaos.

We zoom now the area around the 8/1 and 9/1 secondary resonances. Figs. 7 and 8 show  $f_\varpi$  versus semi-major axis. The determination is done on the basis of  $4 \times 10^5$  yr numerical integrations of each initial condition ( $e = 0.2168$ ). Jupiter's eccentricity equals 0.048 26 here. Fig. 7 is a libration-island crossing, showing positions of the separatrices at both borders of the flat, almost horizontal area. We amplified the left separatrix (inset) to see if some narrow chaotic zone appears there, but even this additional zoom did not show any irregularities of the frequency map. A discontinuity of the frequency map at a hyperbolic point crossing was observed at the 9/1 secondary resonance (Fig. 8). The zoom revealed a narrow chaotic layer in its vicinity (MLE equals  $10^{-4.5} \text{ yr}^{-1}$  there).

We placed an asteroid inside this layer with initial conditions  $a = 0.625 825 a_J$  and  $e = 0.2168$  and numerically integrated its trajectory over 10 Myr (Fig. 9). The frequencies  $f_\sigma$  and  $f_\varpi$  were denoted by f1 and f2 in the figure. The parameters of FMA used here were the same as the ones used for an investigation of the chaotic diffusion over 10 Myr in the four-body model described in the following section. Error bars are shown in the figure of the  $f_\varpi$  evolution.

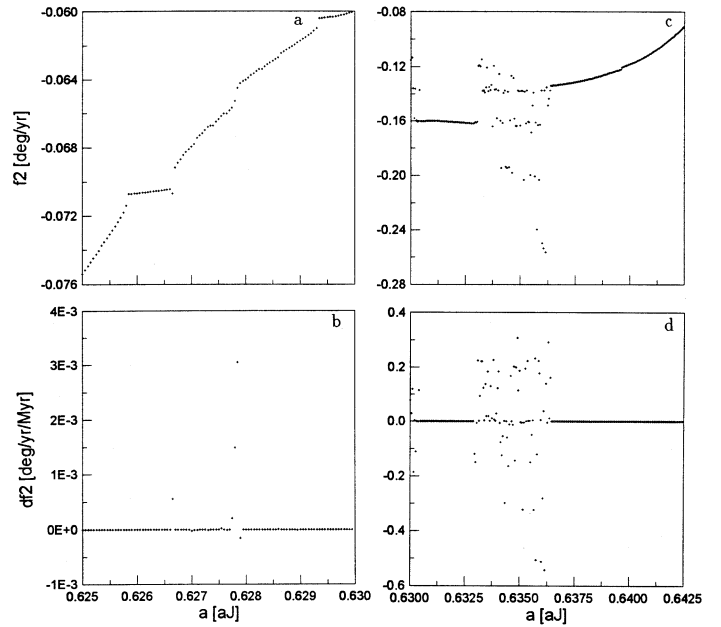


**Fig. 11a–d.** The regularity of motion at  $e = 0.25$  (left) and the confinement of the low-eccentricity chaos at  $e = 0.15$  (right) for  $e_J = 0.061$

At approximately 6 Myr the trajectory switched from one mode to another. This behaviour resembles the one observed in a chaotic trajectory, which is originally at some relatively stable trajectory with a slowly librating resonant angle and then crosses the separatrix and appears in a region of faster circulation. The period visible in the eccentricity evolution corresponds to the period of the resonant angle of the 9/1 secondary resonance, almost 3 Myr at the beginning and slightly less than 1 Myr at the end.

Fig. 10 illustrates a sensitivity of the three-body planar model to the value of Jupiter's eccentricity (the number in the corner of each top figure) in a region close to the low-order secondary resonances. We estimated the temporal frequency variation with an offset of  $2 \times 10^5$  yr (bottom pictures) and  $2T = 4 \times 10^5$  yr. The initial eccentricity of the whole set of the initial conditions is 0.2168.

From left to right we increased Jupiter's eccentricity from 0.048 to 0.061. For  $e_J = 0.048$  the whole region is regular with an exception of a close vicinity of the separatrices of the secondary resonances (as we have seen in Fig. 8). There are some secondary resonances of higher degree between the 8/1 island on the left and the 9/1 hyperbolic point at  $a \sim 0.6278 a_J$ : the small island at  $a \sim 0.6270 a_J$  (resonance 26/3) and the hyperbolic-like crossing at  $a \sim 0.6267 a_J$  (17/2). The secondary resonances become more apparent for  $e_J = 0.053$  and for  $e_J = 0.057$  the area at the right of 8/1 turns chaotic leaving only the small regular island, which is the enlarged 26/3 resonance. For  $e_J = 0.061$  even that one disappears.

But the motion preserves regularity already for  $e = 0.25$  or even for lower eccentricities, as  $e = 0.15$ , at  $a > 0.637 a_J$ . Fig. 11a–d documents this fact with  $e_J = 0.061$ . On the left-hand side of this figure, there is a set of initial conditions with

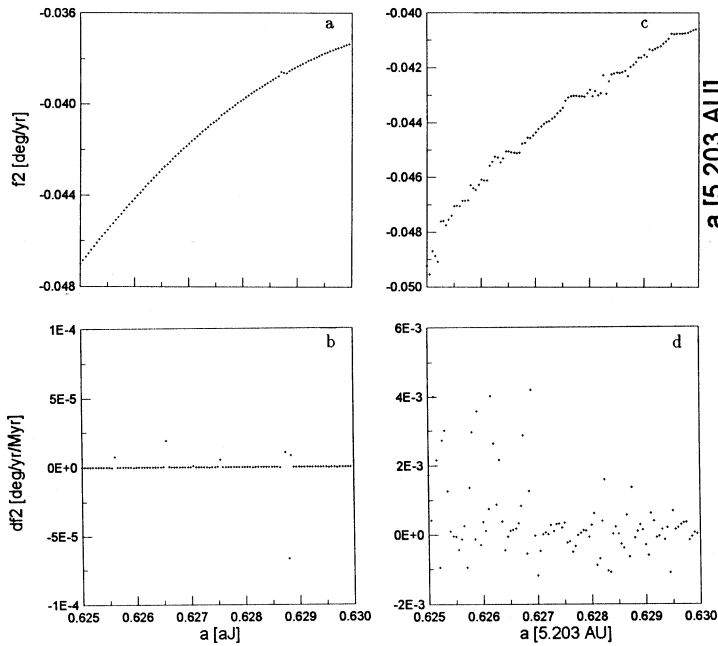


**Fig. 12a–d.** The continuous frequency map vanishes in the four-body model at  $e = 0.3$

$e = 0.25$ , and on the right-hand side, there is another with  $e = 0.15$ . The bottom pictures are changes of the frequency over  $2 \times 10^5$  yr. For  $e = 0.25$  only the strip at  $a \sim 0.628 a_J$  is chaotic ((a) and (b)) and the region  $a > 0.637 a_J$  is perfectly regular for  $e = 0.15$  ((c) and (d)).

## 5. Chaotic diffusion in the four-body model

Fig. 12a–d illustrates a disappearance of the continuous frequency map in the full, four-body planar model. The top figures are, once again, the frequency  $f_\omega$  versus semi-major axis and the bottom figures are the frequency changes over  $2 \times 10^5$  yr. Initial eccentricities are equal to 0.3. The planar three-body model with fixed Jupiter’s orbit ( $e_J = 0.061$ ) is on the left and the planar four-body model with Saturn is on the right. The frequency map is smooth in the three-body model (a). Only slight discontinuities appear at some places due to the high-order secondary resonances and the corresponding frequency changes suggest a presence of chaos near their separatrices (b). On the other hand, the frequency map is irregular in the four-body model (c) and a significant diffusion exists in the whole investigated interval (d). Other similar experiments were done in different regions on the plane  $\sigma = 0$  and  $\varpi = 0$ . All of them showed the significant chaotic diffusion in the four-body model.

We have studied several intermediate three-body models including only some basic frequencies in Jupiter’s orbit. The chaotic diffusion was already present in a wide area of the phase space, when the two main secular frequencies  $g_5$  and  $g_6$  were incorporated in Jupiter’s eccentricity and longitude of perihelion, but it was roughly by one order slower than in the four-body model. The diffusion was significantly accelerated, roughly to the same rate as in the four-body model, when we added the

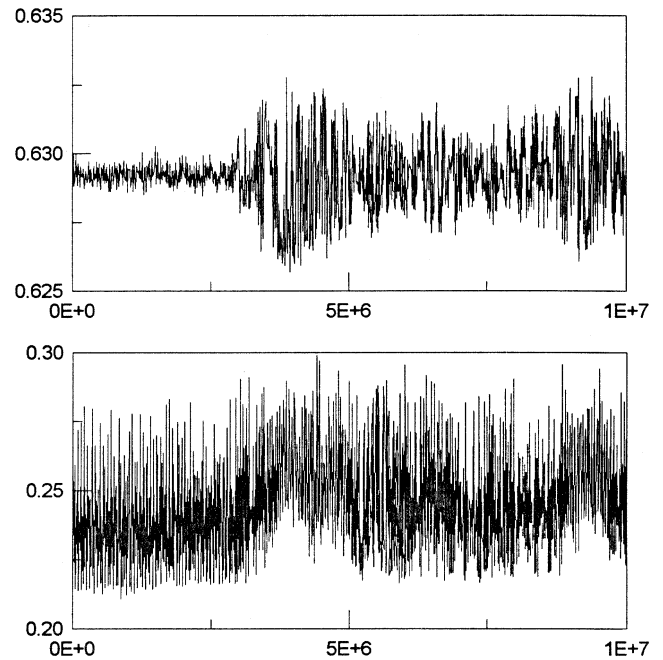


**Fig. 13.** The trajectory with an increasing amplitude of libration

short-periodic terms as well. These short-periodic terms, which are present due to the 2/1 and 5/2 quasi-resonances between Jupiter’s and Saturn’s mean longitudes, seem to play a crucial role in the diffusion acceleration (Ferraz-Mello 1996).

In order to investigate the possible diffusive effect on longer time intervals, we have made numerical integrations with various initial conditions over 10 Myr. Each integration was started with  $\sigma = 0$  and  $\varpi = 0$ . The initial positions of Jupiter and Saturn were projected into the reference plane and turned so that initially  $\lambda_J = 0$ . The frequencies were determined using  $2T = 1$  Myr and shifting the interval with a relatively small offset of  $10^5$  yr along the integration.

In Fig. 13 we show an interesting case of a trajectory initially situated near the libration centers:  $a = 0.63 a_J$  (3.27789 AU) and  $e = 0.217$ . An amplitude of the libration suddenly increased (in this case at 3 Myr), what was observed in several other examples in the neighbouring region.

In Fig. 14 we sum up the results of 16 integrated examples over 10 Myr and plot their diffusion trajectories in the frequency space of  $f_\sigma$  and  $f_\omega$ . The thin lines in the figure are the secondary resonances with  $f_\sigma/f_\omega$  from 6/1 to 10/1. The strong low-eccentricity chaos is located roughly under the 6/1 line (Fig. 2 and Fig. 6). The numbers correspond to each particular initial condition. The diffusion rate ranges from almost zero for the example 8 to values leading to a notable transfer in the frequency space as it can be seen, for instance, in the examples 3 and 10. In the case 3 ( $a = 0.635 a_J$  (3.303 905 AU)), an asteroid crosses the secondary resonances 9/1, 8/1 and 7/1, and almost reaches the low-eccentricity chaotic region. Its eccentricity decreases from initial 0.2 to 0.15. The case 10 is initially placed at  $e = 0.35$  and  $a = 0.625 a_J$  (3.251 875 AU). The  $f_\sigma$  variations are accompanied by changes of the amplitude of the

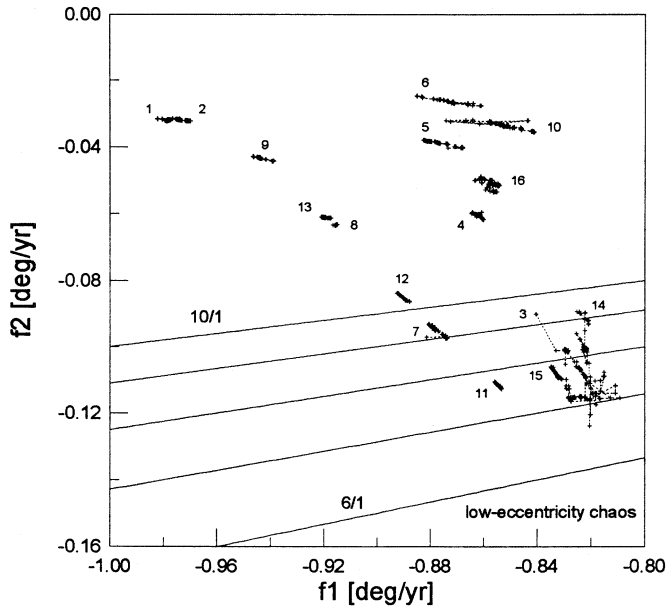


Fig. 14. Chaotic diffusion in the frequency space

semi-major axis oscillations, which decreases to roughly one half of the initial value and the trajectory gets near the libration centers. The moderate diffusion observed in the cases seen approximately along the line connecting the cases 1 and 11 in the figure corresponds to initial conditions far from the librations centers at  $a = 0.62 a_J$  (3.225 86 AU) and  $a = 0.64 a_J$  (3.329 92 AU).

Since each integration over 10 Myr needs several computer hours at a workstation, we have not yet been able to extend the set of initial conditions to a more representative sample. But, at least as a qualitative estimate of the diffusion effect over 1 Gyr, one may suppose, as known for diffusive processes, that the mean displacement depends on the square root of time. Thus, if the phase-space were roughly homogeneous, the extent of each trajectory in Fig. 14 would increase by one order. However, longer numerical integrations showed a complexity of the phase-space and an existence of the slow-diffusion barriers, which often confine a trajectory with a fast diffusion to a small bounded area for a long time.

## 6. Conclusion

We have applied the frequency map analysis on the problem of asteroidal motion in the 2/1 mean-motion resonance with Jupiter. Laskar's technique was adapted for the particular use in this dynamical system. The method was then applied to the planar three-body model. We have shown the most detailed correct reproduction of the low-eccentricity chaotic region and investigated the chaos produced by the high-order secondary resonances. We compared their position with that predicted by the semi-numerical method in the circular problem. The narrow chaotic layers were found to be localized in the vicinity of their separatrices. The region around the low-eccentricity chaos is sensible to the value of Jupiter's eccentricity, the chaos

grown for  $e_J = 0.061$  but still left a great portion of the phase space regular. The regularity disappeared when the variations of Jupiter's orbit were included and the moderate eccentricity region became chaotic. The effect of the slow chaotic diffusion in moderate eccentricities was then studied on the basis of several 10 Myr integrations with Saturn. It has not yet been possible to make any statistic conclusions about the diffusion effect over much longer time spans. But it seems clear, as the observed changes of several integrated trajectories were so important, that a prolongation of the time interval by two orders of magnitude would allow at least some portion of asteroids to enter the fast low-eccentricity chaos or to reach directly the large eccentricities allowing close encounters with the planets.

*Acknowledgements.* The authors are grateful to Dr. M. Šidlichovský, who supplied them with an algorithm of the high-to-low frequency determination technique, and to Dr. C. Beaugé for valuable suggestions to the manuscript. This work was sponsored by the Research Foundation of the State of São Paulo.

## References

- Cohen, C. J., Hubbard, E. C. and Oesterwinter, C., 1973, *Astron. Papers Am. Ephemeris* 22
- Everhart, E., 1985, in *Dynamics of Comets: Their origin and evolution* (eds. A. Carusi and G.B. Valsecchi), p. 185, Reidel, Dodrecht
- Ferraz-Mello, S., 1994, *AJ* 108, 2330
- Ferraz-Mello, S., 1996, in *Proc. IAU Symposium 172* (eds. S. Ferraz-Mello, B. Morando and J.-E. Arlot), p. 177
- Ferraz-Mello, S. and Sato, M., 1989, *A&A* 225, 541
- Giffen, R., 1973, *A&A* 23, 387
- Henrard, J., Watanabe, N. and Moons, M., 1995, *Icarus* 115, 336
- Laskar, J., 1990, *Icarus* 88, 266
- Laskar, J., 1993, *Physica D* 67, 257
- Laskar, J., Froeschlé, C. and Celletti, A., 1992, *Physica D* 56, 253
- Lemaître, A. and Henrard, J., 1990, *Icarus* 83, 391
- Michtchenko, T. and Ferraz-Mello, S., 1995, *A&A* 303, 945
- Michtchenko, T. and Ferraz-Mello, S., 1996, *A&A* 310, 1021
- Moons, M. and Morbidelli, A., 1993, *Celest. Mech. & Dynam. Astron.* 57, 99
- Morbidelli, A. and Moons, M., 1993, *Icarus* 102, 316
- Murray, C. D., 1986, *Icarus* 65, 70
- Quinlan, G. D. and Tremaine, S., 1990, *AJ* 100, 1694
- Press, W. H., Teukolsky, S. A., Vetterling W. T. and Flannery, B. P., 1992, *Numerical Recipes in C*, Cambridge University Press, Cambridge, UK
- Quinn, T. R., Tremaine, S. and Duncan, M., 1991, *AJ* 101, 2287
- Wisdom, J., 1987, *Icarus* 72, 241